Modeling of a spiral-wound reverse osmosis process and parameter estimation

M.A. Al-Obaidi[a,b], C. Kara-Zaitri[a], I.M. Mujtaba[a,*]

[a]*Chemical Enginerring, School of Engineering, Faculty of Engineering and Informatics, University of Bradford, Bradford, BD7 1DP, UK, Tel. +44 0 1274 233645, email: M.A.A.Alobaidi@student.bradford.ac.uk (M.A. Al-Obaidi), C.Karazaitri@bradford.ac.uk (C. Kara-Zaitri), I.M.Mujtaba@bradford.ac.uk(I.M. Mujtaba)*
[b] *Middle Technical University, Iraq - Baghdad*

ABSTRACT

Reverse osmosis system has been widely used for the separation of organic and non-organic pollutants present in wastewater. The main aim of this study is to develop a one dimensional steady state model based on the three-parameter Spiegler-Kedem methodology using the gPROMS software and validate it by assessing the performance of membrane rejection for the separation data of aqueous solutions of phenol under different concentrations and pressures. Considerations of the variance of pressure, flow rate, solute concentration, solvent and solute fluxes and mass transfer coefficient along the feed channel were included in the model. Furthermore, an optimization methodology for the gEST parameter estimation tool has been developed in the gPROMS and used with experimental data in order to estimate the best values of the separation membrane parameters and the friction parameter. The simulation results of this model have been corroborated by experimental data.

Keywords: Reverse osmosis; Spiral-wound; One dimensional-model; gPROMS; Parameter estimation; Wastewater treatment

1. Introduction

Reverse osmosis (RO) has been widely used for the separation of solutes, such as desalination of seawater and industrial effluent treatment where it is able to operate under variable conditions of feed flow rate, pressure and temperature [1–4]. In the past two decades, many models have been reported in the literature for spiral-wound RO configuration for removing organic and non-organic compounds from aqueous solutions. Despite the complexity of the different available approaches, only two models are used widely and include the solution-diffusion model [5] and the irreversible thermodynamic model [6]. The solution-diffusion model requires only a few parameters to be known to measure the mechanism of transport compared to that by the irreversible thermodynamic model. However, the interaction between the solute, solvent and membrane

are specifically included in the irreversible thermodynamic model. As a result, this model is more widely used to describe the performance of the membrane separation in RO systems than any other investigated models [7,8].

The available transport models are based on analytical and distributed methodologies. The analytical type assumes constant average conditions in each edge of the membrane while the distributed type uses the spatial variation of operating variables [4]. The literature on modeling the reverse osmosis membrane separation using the irreversible thermodynamic model is discussed in more detail elsewhere [9]. Further literature is addressed in the next section of the paper.

The starting fundamental formula for the irreversible thermodynamic model was established by Kedem and Katchalsky [10] and then by Spiegler and Kedem [11] for a dilute two-component non-electrolyte system of water and solute as linear equations and non-linear equations respectively relating the fluxes of these components. The interesting aspect of this work is the idea that there should

*Corresponding author.

be a combination of three parameters rather than two as assumed in the solution-diffusion model. A third parameter of the reflection coefficient is added in order to express the broad criteria of a sensible interaction between the solute-solvent-membrane, which generates and enhances an acting force between them. Furthermore, it was confirmed that for a dilute single solute system, the reflection coefficient is approximately equal to one for impermeable solute and less than one for permeable solute. The modification of this model is continued and controlled so that it can be suitable for multi-component systems.

Along the same previous concept, Galey and Bruggen [12] extended the Kedem and Katchalsky model to identify a mixture of non-electrolyte dilute solution. They indicated that the flux of each solute affected by other solutes and the solute interaction depends mainly on solute permeability, concentration and molecular size. It is worth noting that the most specific multi-component thermodynamic model was derived by Pusch [13], who improved the underlying equations of Kedem and Katchalsky for predicting solvent flux and solute rejection.

Likewise, Perry and Linder [14] refined the Spiegler and Kedem model in order to be satisfied for a mixture of salt accompanied by an organic ion. The evolution of their modelling was under the presumption of no concentration polarization and constant values for both the permeability and reflection coefficient parameters. Later on, the Spiegler and Kedem model has been combined with the film theory model by Schirg and Widmer [15] to identify the impact of concentration polarization in case there is a relation between permeate and bulk solute concentration.

The validity of the Spiegler and Kedem model has been assessed later by Van Gauwbergen and Baeyens [16]. They concluded that this model can be utilized effectively for high volume flow rates and high concentration gradients.

Based on the irreversible thermodynamic model, all the above concepts have been developed as analytical models. In contrast, there are only a few models, which consider the spatial variation. For example, Ahmad et al. [17] have developed a one-dimensional model to consider the solute-solute interactions in a multi-component system for a nanofiltration process. While, Fujioka et al. [18] have developed a one-dimensional model for a spiral-wound RO process by assuming zero pressure on the permeate side and they have validated this against experimental data of N-nitrosamine rejection.

There is therefore a clear need to develop a new distributed model for a spiral-wound module applicable to wastewater treatment data based on using the principles of the irreversible thermodynamic equations albeit with relaxing the assumption that the pressure on the permeate side is zero.

This paper presents a new explicit one-dimensional steady state model based on the Spiegler and Kedem model for general spiral-wound RO system, which is coded in the gPROMS software package (Process Systems Enterprise, PSE). The model can predict the variation of solute concentration, pressure, flow rate, mass transfer coefficient, solvent and solute fluxes along the length of the feed channel. The gEST parameter estimation tool in the gPROMS software has been utilized with experimental data to estimate the best values of the membrane and the friction parameters. Also, an equation for the mass transfer coefficient is investigated

according to experimental data to show the impact of solvent flux, flow rate, solute concentration and both the solvent and solute properties. The actual data available in the literature about phenol removing from aqueous solutions will be utilized to validate the model and show its robustness.

The process model developed is then used to study the variation of solute concentration, pressure, flow rate, solvent and solute fluxes along the length of the feed channel.

The proposed model can be applied later to investigate the impact of variation in operating conditions on the permeate flux and solute rejection. Additionally, the model can be used for other different arrangements of spiral-wound RO and optimise design and operation parameters and evaluate system performance.

2. Theoretical background

This section outlines the assumptions and process modelling aspects of the proposed methodology.

2.1. The assumptions

The following assumptions were taken to develop the process model:

1. The flat membrane sheet has negligible channel curvature.
2. Validity of the Spiegler-Kedem model.
3. Validity of Darcy's law where the friction parameter is used to characterize the pressure drop.
4. A constant pressure of 1 atm is assumed at the permeate side.
5. A constant solute concentration is assumed in the permeate channel and the average value will be calculated from the inlet and outlet permeate solute concentrations.
6. The model is investigated for simply one-dimensional transport (x- coordinate).
7. The underlying process is assumed to be isothermal.

2.2. Process modeling

According to the Spiegler-Kedem model, the volumetric solvent and molar solute fluxes $J_{w(x)}$ and $J_{s(x)}$ (m/s and k mol/m² s) at each point along the *x*-axis can be described as:

$$J_{w(x)} = L_p \left(\Delta P_{b(x)} - \sigma \Delta \pi_{s(x)} \right) \tag{1}$$

$$J_{s(x)} = J_{w(x)}(1-\sigma)\tilde{C}_{s(av)} + \omega \Delta \pi_{s(x)} \tag{2}$$

where L_p, ω and σ (m/atm s, k mol/m² s atm and dimensionless) are the hydraulic permeability, solute permeability coefficients of the membrane and the reflection coefficient respectively. In addition, $\Delta P_{b(x)}$ and $\Delta \pi_{s(x)}$ (atm) are the trans-membrane and osmotic pressure difference in each point along the membrane length. $\tilde{C}_{s(av)}$ (k mol/m³) is the average solute concentration calculated from:

$$C_{s(av)}^{\sim} = \frac{C_{s(0)}^{\sim} + C_{s(L)}^{\sim}}{2} \tag{3}$$

where,

$$C_{s(0)}^{\sim} = \frac{C_{s(0)} - C_{p(av)}}{\ln\left(\dfrac{C_{s(0)}}{C_{p(av)}}\right)} \quad \text{and} \quad C_{s(L)}^{\sim} = \frac{C_{s(L)} - C_{p(av)}}{\ln\left(\dfrac{C_{s(L)}}{C_{p(av)}}\right)} \tag{4}$$

$C_{s(0)}^{\sim}$, $C_{s(L)}^{\sim}$ and $C_{p(av)}$ are the inlet and outlet average solute concentrations and average permeate solute concentration respectively. While, $C_{s(0)}$ and $C_{s(L)}$ are the inlet and outlet feed solute concentrations in feed channel. The osmotic pressure $\Delta\pi_{s(x)}$ is described as:

$$\Delta\pi_{s(x)} = RT_b\left(C_{w(x)} - C_{p(av)}\right) \tag{5}$$

where R, T_b and $C_{w(x)}$, $\left(\dfrac{\text{atm m}^3}{\text{K kmol}}\right)$ K and k mol/m³) are the gas constant, the brine temperature and the molar solute concentration on the membrane surface respectively. Putting the value of osmotic pressure difference in Eq. (2), and then the solute flux can be written as:

$$J_{s(x)} = J_{w(x)}\left(1-\sigma\right)C_{s(av)}^{\sim} + \omega RT_b\left(C_{w(x)} - C_{p(av)}\right) \tag{6}$$

Eq. (6) expresses the solute flux by incorporating of two terms. The first term illustrates the solute transport mechanism by convection, which is caused by the coupling between the solute and solvent through three parameters, $\sigma C_{s(av)}^{\sim}$ and $J_{w(x)}$. The second term illustrates the diffusive solute flux. In case of assuming no coupling between the solvent and solute, the term of convection will be zero (*the Solution-diffusion model*).

Since the solute flux is lower than volumetric solvent flux, Eq. (7) yields:

$$J_{s(x)} = J_{w(x)}C_{p(av)} \tag{7}$$

The trans-membrane pressure $\Delta P_{b(x)}$ at any point along the *x*-axis can be defined as:

$$\Delta P_{b(x)} = \left(P_{b(x)} - P_p\right) \tag{8}$$

where $P_{b(x)}$ and P_p (atm) are the pressure on the feed and permeate channels respectively.

By substituting Eq. (7) in Eq. (2) and with re-arrangement, yields:

$$\Delta\pi_{s(x)} = \frac{J_{w(x)}C_{p(av)}}{\omega} - \frac{J_{w(x)}\left(1-\sigma\right)C_{s(av)}^{\sim}}{\omega} \tag{9}$$

Then, by substituting Eq. (9) in Eq. (1).

$$J_{w(x)} = L_p\left[\Delta P_{b(x)} - \sigma\left(\frac{J_{w(x)}C_{p(av)}}{\omega} - \frac{J_{w(x)}\left(1-\sigma\right)C_{s(av)}^{\sim}}{\omega}\right)\right] \tag{10}$$

Eq. (10) can be simplified to:

$$J_{w(x)} = \frac{L_p\left(\Delta P_{b(x)}\right)}{1 + \dfrac{\sigma C_{p(av)}L_p}{\omega} - \dfrac{C_{s(av)}^{\sim}\left(1-\sigma\right)L_p\sigma}{\omega}} \tag{11}$$

Primarily, the brine flow rate $F_{b(x)}$ (m³/s) decreases along the membrane length, which can be estimated from:

$$\frac{dF_{b(x)}}{dx} = -WJ_{w(x)} \tag{12}$$

where $W(m)$ is the width of the membrane.

By combining Eq. (10) in Eq. (12) and take the first and second derivatives yields:

$$\frac{d^2F_{b(x)}}{dx^2} = \frac{-WL_p\dfrac{dP_{b(x)}}{dx}}{1 + \dfrac{\sigma C_{p(av)}L_p}{\omega} - \dfrac{C_{s(av)}^{\sim}\left(1-\sigma\right)L_p\sigma}{\omega}} \tag{13}$$

Then, Darcy's law can be used to express the pressure drop along the membrane length, which is caused by the wall friction along the membrane:

$$\frac{dP_{b(x)}}{dx} = -bF_{b(x)} \tag{14}$$

where b (atm s/m⁴) is the friction factor along the feed channel.

By substituting Eq. (14) in Eq. (13).

$$\frac{d^2F_{b(x)}}{dx^2} = \frac{WL_{pb}F_{b(x)}}{1 + \dfrac{\sigma C_{p(av)}L_p}{\omega} - \dfrac{C_{s(av)}^{\sim}\left(1-\sigma\right)L_p\sigma}{\omega}} \tag{15}$$

Eq. (15) can be composed in the same form of Eq. (16):

$$\frac{d^2F_{b(x)}}{dx^2} = \frac{L_p}{Z}F_{b(x)} \tag{16}$$

where

$$Z = \frac{1 + \dfrac{\sigma C_{p(av)}L_p}{\omega} - \dfrac{C_{s(av)}^{\sim}\left(1-\sigma\right)L_p\sigma}{\omega}}{Wb} \tag{17}$$

The general solution of Eq. (16) is:

$$F_{b(x)} = e^{rx} \text{ where, } r = \pm\sqrt{\frac{L_p}{Z}} \tag{18}$$

The boundary conditions can be used to find the final solution as follows:
At $x=0$, $F_{b(x)} = F_{b(0)}$ and at $x = L$, $F_{b(x)} = F_{b(L)}$

$$F_{b(x)} = \frac{F_{b(L)}\left(e^{\sqrt{\frac{L_p}{Z}}x} - e^{-\sqrt{\frac{L_p}{Z}}x}\right) + F_{b(0)}\left(e^{\sqrt{\frac{L_p}{Z}}(L-x)} - e^{-\sqrt{\frac{L_p}{Z}}(L-x)}\right)}{\left(e^{\sqrt{\frac{L_p}{Z}}L} - e^{-\sqrt{\frac{L_p}{Z}}L}\right)} \tag{19}$$

By substituting Eq. (19) in Eq. (14) and take the integration yields:

$$P_{b(x)} = P_{b(0)} - \frac{b}{\sqrt{\frac{L_p}{Z}}\left(e^{\sqrt{\frac{L_p}{Z}}L} - e^{-\sqrt{\frac{L_p}{Z}}L}\right)}$$

$$\left\{\left[\left[F_{b(L)}\left[e^{\sqrt{\frac{L_p}{Z}}x} + e^{-\sqrt{\frac{L_p}{Z}}x} - 2\right]\right.\right.\right.\tag{20}$$
$$\left.\left.\left.- F_{b(0)}\left[\left(e^{\sqrt{\frac{L_p}{Z}}(L-x)} + e^{-\sqrt{\frac{L_p}{Z}}(L-x)}\right) - \left(e^{\sqrt{\frac{L_p}{Z}}L} - e^{-\sqrt{\frac{L_p}{Z}}L}\right)\right]\right]\right]\right\}$$

Then, by taking the first derivative of Eq. (19) and combine it in Eq. (12), yields:

$$J_{w(x)} = \frac{\sqrt{\frac{L_p}{Z}}}{W\left(e^{\sqrt{\frac{L_p}{Z}}L} - e^{-\sqrt{\frac{L_p}{Z}}L}\right)}$$

$$\left\{\left[F_{b(0)}\left(e^{\sqrt{\frac{L_p}{Z}}(L-x)} + e^{-\sqrt{\frac{L_p}{Z}}(L-x)}\right)\right] - \left[F_{b(L)}\left(e^{\sqrt{\frac{L_p}{Z}}x} + e^{-\sqrt{\frac{L_p}{Z}}x}\right)\right]\right\}\tag{21}$$

By equating Eq. (21) to Eq. (11), the pressure drop along the *x*-axis can be written as:

$$\Delta P_{b(x)} =$$
$$\frac{\sqrt{\frac{L_p}{Z}}Zb\left\{\left[F_{b(0)}\left(e^{\sqrt{\frac{L_p}{Z}}(L-x)} + e^{-\sqrt{\frac{L_p}{Z}}(L-x)}\right)\right] - \left[F_{b(L)}\left(e^{\sqrt{\frac{L_p}{Z}}x} + e^{-\sqrt{\frac{L_p}{Z}}x}\right)\right]\right\}}{L_p\left(e^{\sqrt{\frac{L_p}{Z}}L} - e^{-\sqrt{\frac{L_p}{Z}}L}\right)}\tag{22}$$

Simply at ($x = 0$, $\Delta P_{b(x)} = \Delta P_{b(0)} = P_{b(0)} - P_p$), Eq. (22) can be re-arranged to find an expression for the outlet brine flow rate:

$$F_{b(L)} = \frac{F_{b(0)}\left(e^{\sqrt{\frac{L_p}{Z}}L} + e^{-\sqrt{\frac{L_p}{Z}}L}\right)}{2} - \frac{\Delta P_{b(0)}\sqrt{\frac{L_p}{Z}}\left(e^{\sqrt{\frac{L_p}{Z}}L} + e^{-\sqrt{\frac{L_p}{Z}}L}\right)}{2b}\tag{23}$$

The solute concentration along the x-axis can be calculated from Eq. (24) [19].

$$\frac{d\frac{\left(C_{s(x)}F_{b(x)}\right)}{t_f W}}{dx} = -\frac{J_{w(x)}C_{p(av)}}{t_f} + \frac{J_{w(x)}C_{s(x)}}{t_f} + \frac{d}{dx}\left(D_{b(x)}\frac{dC_{s(x)}}{dx}\right)\tag{24}$$

where $D_{b(x)}$, t_f (m²/s, m) are the solute diffusion coefficient along the length of the membrane (varied with temperature and solute concentration) and the channel height respectively.

Additionally, in order to address the accumulation of the impermeable solute on the membrane surface, the theory of concentration polarization can be applied:

$$\frac{\left(C_{w(x)} - C_{p(av)}\right)}{\left(C_{s(x)} - C_{p(av)}\right)} = \exp\left(\frac{J_{w(x)}}{k_{(x)}}\right)\tag{25}$$

where $k_{(x)}$ (m/s) is the mass transfer coefficient of the solute along the *x*-axis. The combination of Eq. (25) and Eq. (7) in Eq. (2), yields:

$$J_{w(x)}C_{p(av)} = \tilde{C}_{s(av)}(1-\sigma)J_{w(x)} + \omega RT_b\left(C_{s(x)} - C_{p(av)}\right)e^{\frac{J_{w(x)}}{k_{(x)}}}\tag{26}$$

Re-arranging Eq. (26) for the average permeate solute concentration gives:

$$C_{p(av)} = \frac{\tilde{C}_{s(av)}(1-\sigma)J_{w(x)} + \omega RT_bC_{s(x)}\,e^{\frac{J_{w(x)}}{k_{(x)}}}}{J_{w(x)} + \omega RT_b\,e^{\frac{J_{w(x)}}{k_{(x)}}}}\tag{27}$$

To simplify Eq. (27), the reflection coefficient will be assumed as ($\sigma = 1$), then:

$$C_{p(av)} = \frac{\omega RT_bC_{s(x)}\,e^{\frac{J_{w(x)}}{k_{(x)}}}}{J_{w(x)} + \omega RT_b\,e^{\frac{J_{w(x)}}{k_{(x)}}}}\tag{28}$$

Then, Eq. (28) can be re-written in the form of Eq. (29) and to be compatible with the case of calculating the average permeate solute concentration from considering the Solution-diffusion model.

$$C_{p(av)} = \frac{B_sC_{s(x)}\,e^{\frac{J_{w(x)}}{k_{(x)}}}}{J_{w(x)} + B_s\,e^{\frac{J_{w(x)}}{k_{(x)}}}}\tag{29}$$

where B_s is the solute permeability coefficient used in the Solution-diffusion model. Then, Eq. (29) can be used in both ($x = 0$ and $x = L$) and then take the average value as the average solute concentration in the permeate channel.

The average solute rejection coefficient, which is a measure of the separation efficiency of the membrane is calculated from [20]:

$$Rej_{(av)} = \frac{C_{s(L)} - C_{p(av)}}{C_{s(L)}} \times 100\tag{30}$$

Lastly, the total permeated flow rate can be calculated from the sum of all permeated water along the *x*-axis:

$$\frac{dF_{p(x)}}{dx} = WJ_{w(x)}\tag{31}$$

$$F_{p(Total)} = F_{p(L)}\tag{32}$$

2.3. Parameter estimation

Before the proposed model can be applied to simulate the operation of a spiral-wound RO process, all the associated parameters must be assigned fixed values. The model has five parameters; namely L_p, ω, B_s, σ and b.

Generally, the parameters of the Spiegler-Kedem model can be predicted by fitting the experimental data with the predicted values for this model. Murthy and Gupta [8] have used

the non-linear parameter estimation method of the Box-Kane-masu to find the model parameters. While, Senthilmurugan et al. [21] have adopted the simplex search method.

In this paper, another way has been used in order to estimate the unknown parameters, which can be executed automatically within the gPROMS parameter estimation (Process System Enterprise Ltd.) [22] for each set of experiments. Obviously, for any given set of values of the unknown parameters, the model equations can be solved to show the unit behaviour at the experimental conditions, therefore yielding the objective function. The optimization of these parameters is achieved by fitting the experimental data shown in Table 3 to the model predicted values by varying certain model parameters in order to maximise the probability that the model will closely predict. The mathematical way used to minimize the objective function is the sum of square errors (SSE) between the experimental outlet concentration, outlet flow rate, total permeated water, outlet pressure and average solute rejection and the calculated values. This can be achieved by altering the model parameters from an initial guesstimate value to optimal values—usually referred to as the optimisation solver. The gPROMS provides a mathematical solver called as MXLKHD, which is based on maximum likelihood optimisation. The optimization problem is posed as a non-linear programming (NLP) problem and is solved using a successive quadratic programming (SQP) method within the gPROMS software [23].

Given: Time invariant controls including, $C_{s(0)}$, $F_{b(0)}$, $P_{b(0)}$ and T_b

Measured variables data ($C_{s(L)}$, $C_{p(av)}$, $F_{b(L)}$, $F_{p(Total)}$, $P_{b(L)}$ and $Rej_{(av)}$

The statistical variance models to be used for the measured variables.

The complete specification of a parameter estimation problem requires:

Obtaining: (L_p, ω, B_s, σ and b).

Minimizing: The sum of square errors (SSE).

For example, (SSE) for the outlet solute concentration is:

$$SSE = \sum_{i=1}^{N_{Data}} \left[C_{s,i}^{Exp.} - C_{s,i}^{Cal.} \right]^2 \tag{33}$$

With the above subject to: Process parameter constraints.

The total results of the parameter estimation were given in Table 1 and show the variation of transport parameters with the inlet feed solute concentration.

It is worth noting the mass transfer coefficient is basically affected by the solvent flux, flow rate, solute concentration and both the solvent and solute properties [24]. Also, the mass transfer coefficient varies along the x-axis dimension. So, the impact of all these factors can be correlated in Eq. (34) as follows:

$$Sh_{(x)} = c_1 \left[Re_{p(x)} Re_{f(x)} C_{m(x)} Sc_{p(x)} Sc_{f(x)} \right]^{c_2} \tag{34}$$

where, $Sh = \dfrac{2 t_f k_{(x)}}{D_{b(x)}} \tag{35}$

$$Re_{p(x)} = \dfrac{2 t_p \rho_{p(x)} J_{w(x)}}{\mu_{p(x)}} \quad \text{and} \quad Re_{f(x)} = \dfrac{2 \rho_{f(x)} F_{b(x)}}{W \mu_{f(x)}} \tag{36}$$

Table 1
The results of parameter estimation

$C_{s(0)} \times 10^3$	$P_{b(0)}$	T_b	$L_p \times 10^6$	$\omega \times 10^6$	$B_s \times 10^6$
2.125	4.93	32.5	1.4045	5.2388	1.7342
2.125	6.9	33.1	1.4045	5.2388	1.7342
2.125	8.9	33.0	1.4045	5.2388	1.7342
2.125	10.9	33.2	1.4045	5.2388	1.7342
2.125	14.8	34.0	1.4045	5.2388	1.7342
4.25	4.93	32.2	1.2483	0.67797	1.0707
4.25	6.9	32.8	1.2483	0.67797	1.0707
4.25	8.9	33.5	1.2483	0.67797	1.0707
4.25	10.9	33.9	1.2483	0.67797	1.0707
4.25	12.8	34.5	1.2483	0.67797	1.0707
4.25	14.8	34.5	1.2483	0.67797	1.0707
6.375	4.93	32.5	1.1314	1.5213	0.84163
6.375	6.9	33.0	1.1314	1.5213	0.84163
6.375	8.9	33.2	1.1314	1.5213	0.84163
6.375	10.9	33.5	1.1314	1.5213	0.84163
6.375	12.8	33.8	1.1314	1.5213	0.84163
6.375	14.8	34.0	1.1314	1.5213	0.84163
8.5	4.93	32.0	1.2090	1.8588	1.1476
8.5	6.9	32.5	1.2090	1.8588	1.1476
8.5	8.9	32.8	1.2090	1.8588	1.1476
8.5	10.9	33.0	1.2090	1.8588	1.1476
8.5	12.8	33.2	1.2090	1.8588	1.1476
8.5	14.8	33.5	1.2090	1.8588	1.1476
10.6	4.93	31.5	1.1184	0.58853	1.0972
10.6	6.9	32.2	1.1184	0.58853	1.0972
10.6	8.9	32.6	1.1184	0.58853	1.0972
10.6	10.9	32.8	1.1184	0.58853	1.0972
10.6	12.8	32.8	1.1184	0.58853	1.0972
10.6	14.8	33.0	1.1184	0.58853	1.0972
b = 13,000 atm s/m⁴				σ = 0.9075	

$$C_{m(x)} = \dfrac{C_{s(x)}}{\rho_m} \tag{37}$$

$$Sc_{p(x)} = \dfrac{\mu_{p(x)}}{\rho_{p(x)} D_{p(x)}} \quad \text{and} \quad Sc_{f(x)} = \dfrac{\mu_{f(x)}}{\rho_{f(x)} D_{f(x)}} \tag{38}$$

where $Sh_{(x)}$, $Re_{p(x)}$, $Re_{f(x)}$, $C_{m(x)}$, $Sc_{p(x)}$, $Sc_{f(x)}$, $\rho_{p(x)}$, $\rho_{f(x)}$, $\mu_{p(X)}$, $\mu_{f(x)}$, $D_{p(x)}$ and ρ_m are the Sherwood number, the permeate Reynolds number, the feed Reynolds number, dimensionless solute concentration, the permeate Schmidt number, the feed Schmidt number, the density of permeate, the density of feed, the viscosity of permeate, the viscosity of the feed, the solute diffusion coefficient of permeate at any point along the x-axis and the molal density of water respectively. In

order to determine the values of (c_1 and c_2) mentioned in Eq. (34), the mass transfer coefficients will be calculated from the correlation reported by Wankat [25].

$$k_{(x)} = 1.177 \left(\frac{F_{b(x)} D_{b(x)}^2}{t_f^2 W L} \right)^{0.333} \tag{39}$$

Then, the other parameters of Eq. (34) in both ($x = 0$ and $x = L$) can be estimated from the experimental data of phenol, which reported by Srinivasan [20].

Finally, by plotting $Ln(Sh)$ vs $Ln (Re_p\ Re_f\ C_m\ Sc_p\ Sc_f)$, the values of constants can be found. As a result, the last construction of mass transfer coefficient of phenol is:

$$k_{(x)} = \frac{6.5045 D_{f(x)}^{0.9995}}{t_f} \left(\frac{F_{b(x)} t_p J_{w(x)} C_{s(x)}}{W \rho_m D_{p(x)}} \right)^{0.0005} \tag{40}$$

3. Experimental procedure

The Perma-TFC polyamide RO membrane in a spiral-wound module (supplied by Permionics, Vododara, India) was used by Srinivasan [20]. The characteristics of the spiral-wound module are given in Table 2. The experiments were carried out using binary mixtures of phenol compound in water at five different solute concentrations varying from 2.125×10^{-3} to 10.6×10^{-3} k mol/m³. Also, the pressure varies from 4.93 to 14.8 atm for each set of inlet feed solute concentration under constant feed flow rate 3.333E-4 m³/s. Lastly, the fluid temperature was kept between 31.5 and 34.5°C.

4. Model validation

Table 3 shows the experimental results of phenol removal and the model predictions for five groups of inlet feed solute concentration (each group holding six different inlet feed pressures). Table 3 also depicts the percentage error between the experimental results and the model predictions for a number of model parameters, such as, outlet feed pressure ($P_{b(L)}$), outlet feed flow rate ($F_{b(L)}$), average permeate solute concentration ($C_{p(av)}$), the total volumetric permeated flow rate ($F_{p(Total)}$) and the average solute rejection ($Rej_{(av)}$). The predicted above parameters have been obtained by running the model for different

Table 2
Specification of polyamide membrane module

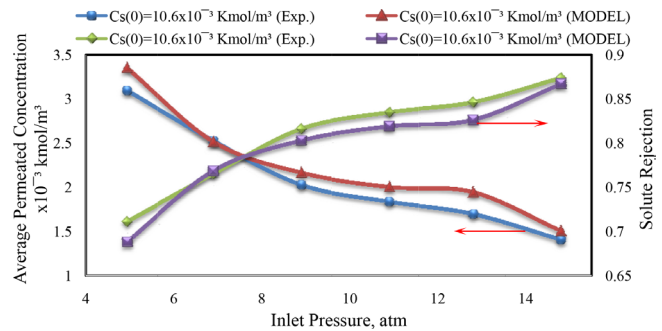| Make	Ion exchange, India
Membrane material	TFC polyamide
Module configuration	Spiral-wound
Number of turns	13
Feed spacer thickness, mm	0.85
Module length, m	0.45
Module width, m	1.6667
Module diameter, inch	2.5

Fig. 1. Comparison of theoretical and experimental results of solute rejection and average permeate concentration.

inlet feed conditions. Fig. 1 shows the comparison of experimental and theoretical results for average solute rejection and average permeate concentration. Generally, the predicted values of the theoretical model are in a good agreement with the experimental ones over the ranges of pressure and concentration.

5. Steady state variation of operating parameters

In steady state mode, Fig 2 shows the variation of feed pressure and concentration along the membrane length. The feed pressure decreases due to pressure drop caused by the friction. As a result, the pressure gradient is at its maximum point at the entrance of membrane and at its minimum point at the end of the unit. While, the feed concentration progresses in the subsequent sub-sections of feed channel since the solute is retained in the wall with the diffusion of water through the membrane.

It is worth noting that the feed flow rate decreases along the membrane channel as can be viewed in Fig. 3 and this can be attributed to the permeated water passing through the membrane, which reduces the velocity of feed and increases the feed concentration along the membrane (Fig. 2).

In addition, the water and solute fluxes decrease along the membrane length as the pressure decreases due to friction which decreases the net pressure driving force as shown in Fig. 4.

Fig. 5 shows that increasing operating pressure results in increasing the solute rejection and total permeated flow rate due to increase in water flux for all the tested feed concentrations. Interestingly, for low inlet feed concentration conditions, the solute rejection increases due to increase in the inlet feed concentration, and this may be attributed to increase in the membrane solute isolation intensity. However, any further increase in inlet feed concentration can cause a reduction in solute rejection due to higher osmotic pressure, which causes a decrease in the driving force of water flux.

6. Conclusions

A one dimensional steady state model based on the theory of the irreversible thermodynamic model has been developed for a spiral-wound RO process based wastewa-

Table 3
Model validation with experimental results for the inlet feed flow rate ($F_{b(0)}$ = 3.333 × 10⁻⁴ m³/s)

| No	$P_{b(0)}$ atm	T_b °C	$C_{s(0)} \times 10^3$ (k mol/m³)	$P_{b(L)}$ (atm)			$Cp_{(av)} \times 10^3$ (k mol/m³)			$F_{p(Total)} \times 10^6$ (m³/s)			$Rej_{(av)}$			$F_{b(L)} \times 10^4$ (m³/s)		
				Exp.	The.	% Error	Exp.	The.	% Error	Exp.	The.	% Error	Exp.	The.	% Error	Exp.	The.	% Error
1	4.93	32.5	2.125	2.99	2.99	0.01	0.831	0.806	3.02	3.53	3.02	14.4	0.6462	0.627	–3.14	3.30	3.30	–0.12
2	6.9	33.1	2.125	4.96	4.97	0.13	0.647	0.637	1.54	5.20	5.18	0.45	0.727	0.708	–2.66	3.28	3.28	–0.00
3	8.9	33	2.125	6.9	6.97	1.04	0.580	0.574	0.96	7.20	7.37	–2.30	0.7593	0.740	–2.62	3.26	3.26	0.03
4	10.9	33.2	2.125	8.9	8.98	0.87	0.524	0.551	–5.17	9.60	9.55	0.48	0.7861	0.753	–4.35	3.24	3.24	–0.06
5	14.8	34	2.125	12.9	12.88	0.15	0.349	0.368	–5.55	12.2	12.2	0.00	0.8745	0.838	–4.37	3.21	3.21	–0.07
6	4.93	32.2	4.25	2.99	2.99	0.00	1.24	1.24	–0.19	3.30	2.68	18.7	0.766	0.712	–7.61	3.30	3.31	–0.16
7	6.9	32.8	4.25	4.96	4.96	0.09	1.05	0.935	5.00	4.60	8.06	0.8132	0.785	–3.54	3.28	3.29	3.29	–0.12
8	8.9	33.5	4.25	6.9	6.97	1.00	0.80	0.81	–1.22	7.00	6.54	6.54	0.861	0.816	–5.46	3.26	3.27	–0.16
9	10.9	33.9	4.25	8.9	8.98	0.84	0.72	0.755	–4.84	8.50	8.49	0.15	0.8737	0.830	–5.21	3.25	3.25	–0.04
10	12.8	34.5	4.25	10.9	10.88	–0.17	0.685	0.73	–6.62	10.25	10.3	–0.82	0.8807	0.838	–5.14	3.23	3.23	–0.03
11	14.8	34.5	4.25	12.9	12.89	0.0	0.718	0.734	–2.20	12.25	12.3	–0.23	0.8766	0.839	–4.53	3.21	3.21	–0.07
12	4.93	32.5	6.375	2.99	2.99	0.00	1.40	1.65	–17.89	3.20	2.43	20.4	0.7983	0.744	–7.22	3.30	3.31	–0.21
13	6.9	33	6.375	4.96	4.96	0.00	1.24	1.21	2.47	4.33	4.17	3.70	0.8216	0.815	–0.86	3.29	3.29	–0.04
14	8.9	33.2	6.375	6.9	6.97	0.98	1.176	1.03	12.15	5.93	5.93	–0.06	0.8346	0.843	1.02	3.27	3.27	–0.02
15	10.9	33.5	6.375	8.9	8.97	0.81	0.94	0.95	–1.05	7.00	7.70	–9.96	0.868	0.857	–1.25	3.26	3.26	0.17
16	12.8	33.8	6.375	10.9	10.9	0.00	0.87	0.913	–4.94	8.70	9.37	–7.73	0.8798	0.864	–1.82	3.25	3.24	0.15
17	14.8	34	6.375	12.9	12.9	0.00	0.63	0.669	–6.12	11.1	11.1	0.00	0.9141	0.902	–1.39	3.22	3.22	–0.07
18	4.93	32	8.50	2.99	2.99	0.00	2.61	2.65	–1.60	3.13	2.60	17.0	0.7061	0.692	–2.00	3.30	3.31	–0.14
19	6.9	32.5	8.50	4.96	4.96	0.08	2.22	2.01	9.64	4.53	4.45	1.68	0.75	0.770	2.54	3.29	3.29	–0.02
20	8.9	32.8	8.50	6.9	6.97	0.99	1.93	1.75	9.58	6.20	6.34	–2.22	0.7834	0.802	2.27	3.27	3.27	0.02
21	10.9	33	8.50	8.9	8.97	0.83	1.60	1.63	–1.94	8.20	8.22	–0.26	0.8261	0.816	–1.18	3.25	3.25	–0.03
22	12.8	33.2	8.50	10.9	10.9	0.00	1.47	1.59	–8.16	9.30	10.0	–7.65	0.8402	0.823	–2.11	3.24	3.23	0.16
23	14.8	33.5	8.50	12.9	12.9	0.00	1.40	1.59	–13.31	11.5	11.9	–3.43	0.8495	0.825	–2.96	3.22	3.22	0.04
24	4.93	31.5	10.6	2.99	2.99	0.00	3.09	3.35	–8.40	2.66	2.40	9.94	0.7112	0.688	–3.38	3.31	3.31	–0.06
25	6.9	32.2	10.6	4.96	4.96	0.00	2.52	2.51	0.39	4.13	4.11	0.47	0.7647	0.768	0.47	3.29	3.29	–0.00
26	8.9	32.6	10.6	6.9	6.97	0.97	2.02	2.16	–6.92	5.86	5.85	0.14	0.8164	0.803	–1.72	3.27	3.28	–0.02
27	10.9	32.8	10.6	8.9	8.97	0.81	1.83	2.00	–9.16	7.50	7.59	–1.24	0.8351	0.819	–1.95	3.26	3.26	–0.01
28	12.8	32.8	10.6	10.9	10.9	0.00	1.69	1.94	–14.53	9.00	9.25	–2.73	0.8462	0.826	–2.40	3.24	3.24	0.02
29	14.8	33	10.6	12.9	12.9	0.00	1.40	1.50	–7.10	10.5	10.5	–0.44	0.8739	0.867	–0.84	3.23	3.23	–0.06
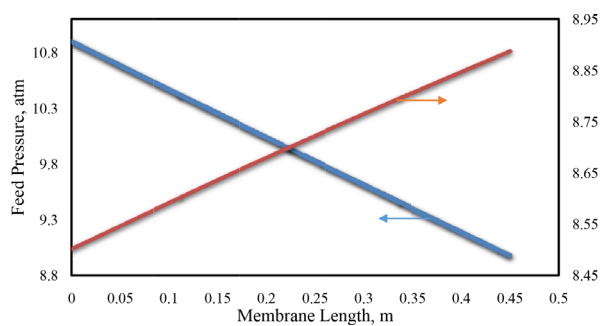
Fig. 2. Feed pressure and concentration variation along the membrane length, inlet feed conditions (3.333 × 10⁻⁴ m³/s, 8.5 × 10⁻³ k mol/m³, 10.9 atm and 32.2°C).

Fig. 3. Feed and permeate flow rates variation along the membrane length, inlet feed conditions (3.333 × 10⁻⁴ m³/s, 8.5 × 10⁻³ k mol/m³, 10.9 atm and 32.2°C).

Fig. 4. Water and solute fluxes variation along the membrane length, inlet feed conditions (3.333×10^{-4} m³/s, 8.5×10^{-3} k mol/m³, 10.9 atm and 32.2°C).

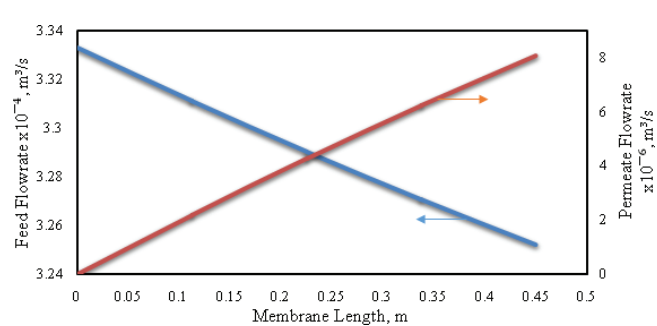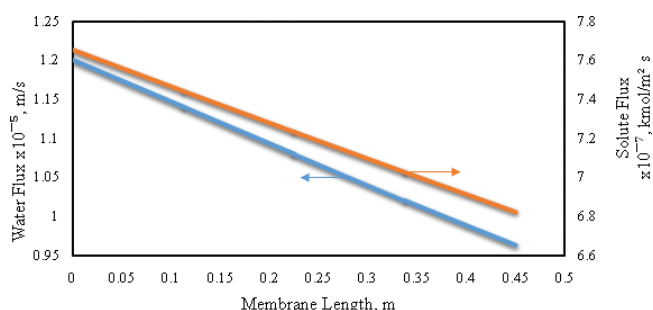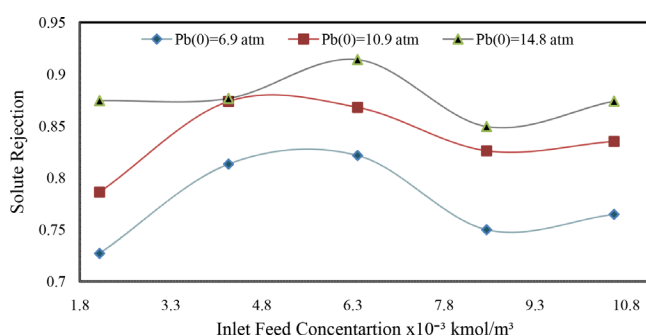Fig. 5. Solute rejection verses inlet feed concentration for three different inlet feed pressure, inlet feed conditions 3.333×10^{-4} m³/s and (32.2–34.5°C).

ter treatment. The model can be used to predict the variation of the operating parameters along the x-axis of the feed channel. The model has been solved using the gPROMS and validated with the experimental data of binary aqueous solutions of phenol derived from the literature. Analysis of the results readily show that the proposed model can be used to simulate phenol rejection for a scaled-up plant with an acceptable convergence with a maximum 7% difference between the theoretical and experimental results. The results show that the solute rejection increases with increasing operating pressure and is mainly dependent on the operating feed concentration. The proposed model can be used further to provide more accurate results for the design of RO process.

Symbols

b	—	Feed channels friction parameter (atm s/m⁴)
B_s	—	The solute permeability coefficients of the membrane, (the Solution-diffusion model) (m/s)
c_1, c_2	—	Constants in Eq. (34)
$C_{m(x)}$	—	Dimensionless solute concentration at any point along the membrane length
C_s	—	Brine solute concentration in the feed channel (k mol/m³)
$\tilde{C}_{s(av)}$	—	The mean solute concentration in the feed side (k mol/m³)
$C_{p(av)}$	—	Average permeate solute concentration in the permeate channel (k mol/m³)
$C_{w(x)}$	—	Solute concentration at the membrane wall at any point along the membrane length, (k mol/m³)
$D_{b(x)}$	—	Diffusivity coefficient of feed at any point along the membrane length (m²/s)
$D_{p(x)}$	—	Diffusivity coefficient of permeate at any point along the membrane length (m²/s)
$F_{b(x)}$	—	Feed flow rate at any point along the membrane length (m³/s)
$F_{p(x)}$	—	Permeate flow rate at any point along the membrane length (m³/s)
$F_{p(Total)}$	—	Total permeated flow rate of the permeate channel (m³/s)
$J_{s(x)}$	—	Solute molar flux through the membrane at any point along the membrane length, (k mol/m² s)
$J_{w(x)}$	—	Water flux at any point along the membrane length (m/s)
$k_{(x)}$	—	Mass transfer coefficient at any point along the membrane length (m/s)
L	—	Length of the membrane (m)
L_p	—	Solvent transport coefficient (m/atm s)
$P_{b(x)}$	—	Feed channel pressure at any point along the membrane length (atm)
P_p	—	Permeate channel pressure (atm)
R	—	Gas low constant
r	—	Parameter defined in Eq. (18)
$Re_{f(x)}$	—	The feed Reynolds number at any point along the membrane length (dimensionless)
$Rej_{(av)}$	—	Solute rejection coefficient (dimensionless)
$Re_{p(x)}$	—	The permeate Reynolds number at any point along the membrane length (dimensionless)
$Sc_{f(x)}$	—	The feed Schmidt number at any point along the membrane length (dimensionless)
$Sc_{p(x)}$	—	The permeate Schmidt number at any point along the membrane length (dimensionless)
$Sh_{(x)}$	—	Sherwood number at any point along the membrane length (dimensionless)
SSE	—	The sum of square errors
T_b	—	Feed temperature (°C)
t_f	—	Feed spacer thickness (m)
W	—	Width of the membrane (m)
x	—	Any point along the membrane length
Z	—	Parameter defined in Eq. (17)

Subscripts

$\rho_{f(x)}$	—	Feed density at each point along the membrane length (kg/m³)
ρ_m	—	The molal density of water (55.56 k mol/m³)
$\rho_{p(x)}$	—	Feed density at each point along the membrane length (kg/m³)
$\mu_{f(x)}$	—	Feed viscosity at each point along the membrane length (kg/m s)
$\mu_{p(x)}$	—	Feed viscosity at each point along the membrane length (kg/m s)

σ	—	The reflection coefficient (dimensionless)
ω	—	The solute permeability coefficients of the membrane (k mol/m² s atm)
Δx	—	Length of the sub-section (m)
$\Delta P_{b(x)}$	—	Trans-membrane pressure at each point along the membrane length (atm)
$\Delta \pi_{s(x)}$	—	The osmotic pressure difference at each point along the membrane length (atm)

References

[1] Y. Yoon, R.M. Lueptow, Removal of organic contaminants by RO and NF membranes, J. Membr. Sci., 261 (1–2) (2005) 76–86.

[2] K.M. Sassi, I.M. Mujtaba, Optimal operation of RO system with daily variation of freshwater demand and seawater temperature, Comp. Chem. Eng., 59 (2013) 101–110.

[3] M. Barello, D. Manca, R. Patel, I.M. Mujtaba, Operation and modeling of RO desalination process in batch mode, Comp. Chem. Eng., 83 (2015) 139–156.

[4] M.A. Al-Obaidi, I.M. Mujtaba, Steady state and dynamic modeling of spiral wound wastewate reverse osmosis process, Comp. Chem. Eng., 90 (2016) 278–299.

[5] H.K. Lonsdale, U. Merten, R.L. Riley, Transport properties of cellulose acetate osmotic membranes, J. Appl. Polym. Sci., 9 (4) (1965) 1341–1362.

[6] K.S. Spiegler, O. Kedem, Thermodynamics of hyperfiltration (reverse osmosis): criteria for efficient membranes, Desalination, 1 (1966) 311–326.

[7] E.A. Mason, H.K. Lonsdale, Statistical-mechanical theory of membrane transport, J. Membr. Sci., 51 (1990) 1–81.

[8] Z.V.P. Murthy, S.K. Gupta, Thin film composite polyamide membrane parameters estimation for phenol-water system by reverse osmosis, Separ. Sci. Technol., 33 (16) (1998) 2541–2557.

[9] S. Sobana, R.C. Panda, Review on modelling and control of desalination system using reverse osmosis, Rev. Environ. Sci. Biotechnol., 10 (2) (2011) 139–150.

[10] O. Kedem, A. Katchalsky, Thermodynamic analysis of the permeability of biological membranes to non-electrolytes, Biochim. Biophys. Acta., 27 (1958) 229–246.

[11] K.S. Spiegler, O. Kedem, Thermodynamics of hyperfiltration (reverse osmosis): criteria for efficient membranes, Desalination, 1 (1966) 311–326.

[12] W.R. Galey, J.T. Bruggen, The coupling of solute fluxes in membranes, J. Gen. Physiol., 55 (2) (1970) 220–242.

[13] W. Pusch, In: Proc. 7th International Symposium on Fresh Water from the Sea, 2 (1980) 207.

[14] M. Perry, C. Linder, Intermediate reverse osmosis ultrafiltration (RO UF) membranes for concentration and desalting of low molecular weight organic solutes, Desalination, 71 (1989) 233–245.

[15] P. Schirg, F. Widmer, Characterisation of nanofiltration membranes for the separation of aqueous dye-salt solutions, Desalination, 89 (1992) 89–107.

[16] D.V. Gauwbergen J. Baeyens, Modelling reverse osmosis by irreversible thermodynamics, Separ. Purif. Technol., 13 (2) (1998) 117–128.

[17] A.L. Ahmad, M.F. Chong, S. Bhatia, Mathematical modeling and simulation of the multiple solutes system for nanofiltration process, J. Membr. Sci., 253 (2005) 103–115.

[18] T. Fujioka, S.J. Khan, J.A. Mcdonald, A. Roux, Y. Poussade, J.E. Drewes, L.D. Nghiem, Modelling the rejection of N-nitrosamines by a spiral-wound reverse osmosis system: Mathematical model development and validation, J. Membr. Sci., 454, (2014) 212–219.

[19] C. Lee, Y. Chen, G. Wang, A dynamic simulation model of reverse osmosis desalination systems, The 5th International Symposium on Design, Operation and Control of Chemical Processes, PSE ASIA, Singapore (2010).

[20] G. Srinivasan, S. Sundaramoorthy, D.V.R. Murthy, Spiral wound reverse osmosis membranes for the recovery of phenol compounds-experimental and parameter estimation studies, Amer. J. Eng. Appl. Sci., 3 (1) (2010) 31–36.

[21] S. Senthilmurugan, A. Ahluwalia, S.K. Gupta, Modeling of a spiral-wound module and estimation of model parameters using numerical techniques, Desalination, 173 (2005) 269–286.

[22] Process System Enterprise Ltd., gPROMS Introductory User Guide. London: Process System Enterprise Ltd., 2001.

[23] A.T. Jarullah, I.M. Mujtaba, A.S. Wood, Kinetic parameter estimation and simulation of trickle-bed reactor for hydrodesulfurization of crude oil, Chem. Eng. Sci., 66 (5) (2011) 859–871.

[24] S. Sundaramoorthy, G. Srinivasan, D.V.R. Murthy, An analytical model for spiral wound reverse osmosis membrane modules: Part II — Experimental validation, Desalination, 277 (2011) 257–264.

[25] P.C. Wankat, Rate-controlled separations. 1st Edn., Springer, 1990, pp: 873, ISBN: 10:1851665218.